Global Scientific JOURNALS

GSJ: Volume 12, Issue 2, February 2024, Online: ISSN 2320-9186

www.globalscientificjournal.com

ELEMENTAL GEOCHEMISTRY OF THE AWAINAT WANIN FORMATION IN THREE SELECTED AREAS, MURZUQ BASIN, SW LIBYA

Osama Rahil Shaltami

Department of Earth Sciences, Faculty of Science, University of Benghazi, Libya

osama.rahil@yahoo.com

Abstract

Evaluating the elemental geochemistry of the exposed rocks of the Awainat Wanin Formation in the Idri, Sabha, and Al Fuqaha sheets, Murzuq Basin, SW Libya, was the goal of this work. The studied formation consists of clastic rocks (sandstone, claystone, siltstone, conglomerate (bone bed), and ironstone). The findings indicated that quartzarenite is the classification for the sandstones of the Idri Sheet, whereas the Sabha Sheet's sandstones are classified into several types, including litharenite, sublitharenite, subarkose, and quartzarenite. Both sublitharenite and subarkose sandstones are found in the Al Fuqaha Sheet. The ironstones are of the Clinton variety. They mostly originated from hydrogenous source. Phosphorite rock is the category for the conglomerate bed. The source of the Awainat Wanin Formation is a mixture of felsic, intermediate, and mafic rocks. It is possible that the studied formation originated from the igneous rocks exposed in the Al Haruj Al Abyad Sheet. The paleoweathering intensity in source area ranges from very slight to extreme. There were variations in both aridity and humidity throughout the deposition. Both immature and mature sediments are present. The deltaic environment with suboxic condition is the confirmed depositional setting for the formation. During deposition the water turned from brackish to fresh. The paleoproductivity varies greatly. The proven paleotectonic settings include active continental margin and passive margin.

Keywords: Elemental Geochemistry, Provenance, Depositional Environment, Paleoweathering, Paleoclimate, Maturity, Paleoproductivity, Paleotectonic Setting, Awainat Wanin Formation, Libya.

1. Introduction

Lelubre (1946) was the first to refer to the Devonian rocks on the Gargaf area as Awainat Wanin Formation. Massa and Collom (1960) adopted these rocks; however, improvements to the definition introduced significant ambiguity. Collomb (1962) proposed the name Chatti Formation for the upper four cycles and limited the Awainat Wanin Formation to the four lower cycles. He also divided the entire Awainat Wanin Formation and the lower portion of the overlying Marar Formation into eight cycles. Massa and Moreau-Benoit (1976) changed the status of the Awainat Wanin Formation to the Awainat Wanin Group, divided into four formations (Awainat Wanin Formation I, Awainat Wanin Formation II, Awainat Wanin Formation III and Awainat Wanin Formation IV). Parizek et al., (1984), Seidl and Rohlich (1984) and Woller (1984) suggested new stratigraphic names for the Middle-Late Devonian rocks. They classified the Awainat Wanin Group into six formations (Bir Al Qasr, Idri, Quttah, Dabdab, Tarut, and Ashkidah formations), incorporating the Tahara Formation and the lowermost portion of the Marar Formation. However, the previous classification is no longer used in most stratigraphic works (e.g., Aziz, 2000). The proven depositional setting of the Awainat Wanin Formation is the deltaic environment (Vos, 1981). The paleontological studies indicated a Middle-Late Devonian age for the formation (e.g., Miles, 2001). The Awainat Wanin Formation appears along the boundaries of the Murzuq Basin. It is commonly acknowledged that the Awainat Wanin Formation is also present in the subsurface of the Murzuq, Ghadames, Kufrah, and Cyrenaica basins (Hallett, 2002). In the subsurface, the Basal Devonian Sandstone (BDS) unit is the most important part for the petroleum companies (Echikh, 1998). The different classifications of the Middle-Late Devonian rocks are shown in Fig. 1.

2. Objective

Doing a geochemical assessment of the exposed rocks of the Awainat Wanin Formation in the Idri, Sabha, and Al Fuqaha sheets (Fig. 2) is the main goal of this work. Provenance, depositional environment, paleoweathering, paleoclimate, maturity, paleoproductivity, and paleotectonic setting were all determined using the major oxide data. The Awainat Wanin Formation in the study area mainly contains clastic rocks (Parizek et al., 1984; Seidl and Rohlich, 1984; Woller, 1984). The author believes that this study represents the initial elemental geochemical evaluation of the Awainat Wanin Formation. The prior presumption was based on the published works. Most previous studies have focused on paleontology (e.g., Aziz, 2000; Miles, 2001; Steemans et al.,

2008), stratigraphy and sedimentology (e.g., Vos, 1981; Blanpied and Rubino, 1997; Sutcliffe et al., 2000; Rahuma et al., 2007; Mohamed et al., 2017; Belhaj et al., 2021), mineralogy (e.g., Morton et al., 2011), well logging (e.g., Jabir et al., 2021; Basal et al., 2023), and organic geochemistry (e.g., Echikh, 1998; Aboglila et al., 2018; Riboulleau et al., 2018).

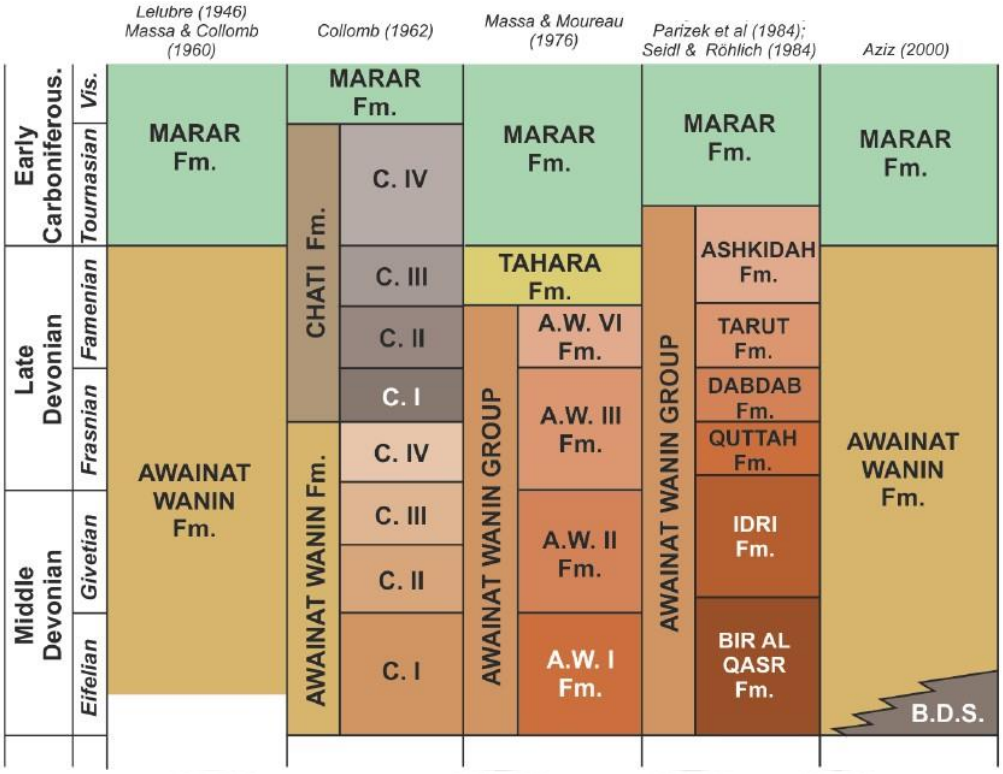

Fig. 1: Different classifications of the Middle-Late Devonian rocks in the Murzuq Basin (after Shalbak, 2015).

3. Methodology

The data used in this work were taken from the Idri, Sabha, and Al Fuqaha sheets (Parizek et al., 1984; Seidl and Rohlich, 1984; Woller, 1984). Fig. 3 shows the location of the studied samples. The rock types are sandstone, mudrocks (claystone and siltstone), conglomerate (bone bed), and ironstone. The total number of the samples is forty one (fifteen samples from the sandstones, nine samples from the mudrocks, one sample from the conglomerate, and sixteen samples from the ironstones). It should be noted that due to the similarity of sample numbers in the studied sheets, the author has modified these numbers in this work to avoid confusion.

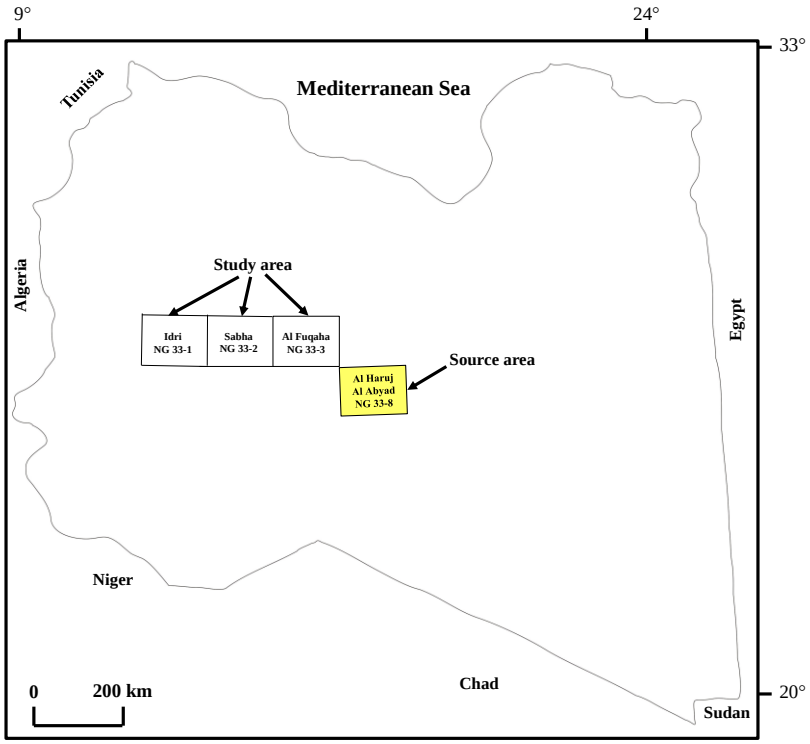

Fig. 2: Map showing the location of the study area and the location of the possible provenance of the Awainat Wanin Formation.

4. Results

The chemical analysis data of the Awainat Wanin Formation in the Idri, Sabha, and Al Fuqaha sheets are shown in Table 1. The following equation was used to determine the FeO concentration: $FeO = 0.8998*Fe_2O_3$. Because of the variations in the lithology, there is a noticeable fluctuation in the concentration of the analyzed major oxides (SiO_2 (5.71-99.02%), TiO_2 (0.06-1.77%), Al_2O_3 (0.01-32.67%), Fe_2O_3 (0.12-68.68%), FeO (0.11-61.8%), MnO (0 -21.2%), MgO (0.08 -2.84%), CaO (0.01 -27.95%), Na_2O (0.05 -6.73%), K_2O (0.02 -1.8%), P_2O_5 (0.02 -25%), SO_3 (0.01 -5.43%), and LOI (0.41-14.2%)).

5. Discussion

5.1. Classification

Several authors have proposed a few classification schemes for sandstone based on the chemical composition (e.g., Pettijohn et al., 1972; Crook, 1974; Herron, 1988). Figs. 4 and 5 indicate that quartzarenite is the confirmed type of the sandstones of the Idri Sheet, while there are different types in the Sabha Sheet, such as quartzarenite, litharenite, sublitharenite, and subarkose. The sandstones of the Al Fuqaha Sheet are classified as sublitharenite and subarkose. Moreover, there

are only four samples in the Sabha Sheet classified as ferruginous sandstone (samples A12, A16, A22, and A28), whereas the former is dominant in the Al Fuqaha Sheet. In addition, the studied sandstones range from quartz-intermediate to quartz-rich (Fig. 6).

The ternary plot of SiO_2-FeO+MgO-Fe_2O_3 (Fig. 7) can be used to differentiate Phanerozoic ironstones from Precambrian iron formations (James, 1992). There are two types of Phanerozoic ironstones: (1) Clinton type; and (2) Minette type (Evans, 1993). The Clinton type is composed of hematite, chamosite, and siderite. Compared to banded iron formation (B.I.F.), the Fe_2O_3 content is between 40 and 50%, and the Al_2O_3 and P_2O_5 contents are higher. Another difference from B.I.F. is the lack of chert bands (SiO_2 is mostly found in iron silicate minerals in trace amounts found in quartz grains). The rocks of the Clinton type ranging in age from Cambrian to Devonian. The most prevalent and widespread type of ironstone is the Minette type. The two main minerals are chamosite and siderite. While CaO ranges from 5 to 20% and SiO_2 is typically above 20%, the Fe_2O_3 content is approximately 30%. The Minette type was prevalent in the Mesozoic and Cenozoic Eras (Evans, 1993). The Fe_2O_3 content in the examined ironstones ranges from 41.72 to 68.68%, which indicates that these rocks belong to the Clinton type. Furthermore, the binary plot of Al versus Si (Fig. 8) suggests a hydrogenous origin of the ironstones. The element values have been recalculated using atomic mass.

Pettijohn (1957) categorized the phosphate bearing rocks into three types based on the P_2O_5 content: (1) Phosphatized rocks (P_2O_5 ranges from 3 to 9.8%); (2) Phosphatic rocks (P_2O_5 ranges from 9.8 to 19.5%); and (3) Phosphorite rocks (P_2O_5 greater than 19.5%). The conglomerate (bone bed) in the Sabha Sheet contains high concentration of P_2O_5 (25%, Table 1), which suggests that this bed is classified as phosphorite rock. The CaO/P_2O_5 ratio is about 1.54 in the pure carbonate fluorapatite (Khan et al., 2012), while the ratio ranges from 3.5 to 5 in the reactive phosphate rock (McClellan and Gremillion, 1980). The CaO/P_2O_5 ratio (1.12) in the conglomerate bed is lower than the previously stated values; which indicates the degree of carbonate substitution in the studied conglomerate.

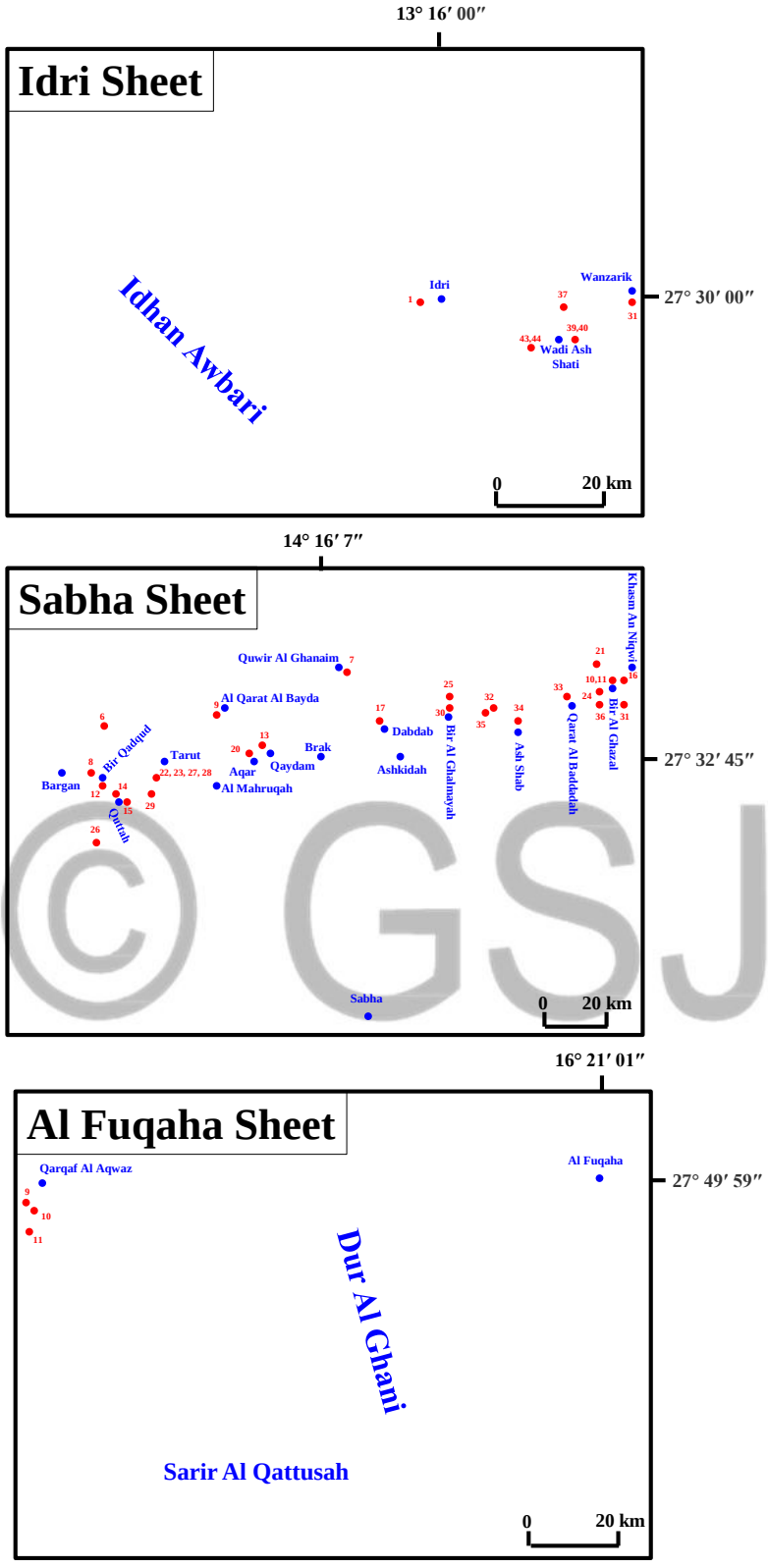

Fig. 3: Maps showing the location of the studied samples (modified after Parizek et al., 1984; Seidl and Rohlich, 1984; Woller, 1984).

Table 1: Chemical analysis data (concentration in wt%) of the Awainat Wanin Formation in the Idri, Sabha, and Al Fuqaha sheets (after Parizek et al., 1984; Seidl and Rohlich, 1984; Woller, 1984)

Sheet	Area	Lithology	Sample No. in the sheets	Sample No. in this work	SiO_2	TiO_2	Al_2O_3	Fe_2O_3	FeO*
Idri	W of Idri	Ironstone	1	A1	24.64	0.45	1.67	57.38	51.63
	SW of Wanzarik	Sandstone	37	A2	95.22	0.08	0.12	1.38	1.24
	NE of Bir Al Qasr	Ironstone	26	A3	22.98	0.63	9.47	41.72	37.54
	ESE of Wanzarik	Sandstone	31	A4	97.63	0.06	0.40	0.25	0.22
	Wadi Ash Shati	Ironstone	39	A5	5.71	0.21	4.15	45.64	41.07
	Wadi Ash Shati	Ironstone	40	A6	6.14	0.45	4.68	62.89	56.59
	Wadi Ash Shati	Ironstone	43	A7	8.58	0.50	5.41	68.68	61.80
	Wadi Ash Shati	Ironstone	44	A8	24.80	0.64	2.28	46.80	42.11
Sabha	NE of Bargan	Claystone	6	A9	42.94	1.15	27.38	9.19	8.27
	Quwir Al Ghanaim	Sandstone	7	A10	97.71	0.06	0.50	0.80	0.72
	SE of Bargan	Sandstone	8	A11	98.56	0.18	0.01	0.33	0.30
	W of Al Qarat Al Bayda	Sandstone	9	A12	90.46	0.25	2.19	3.08	2.77
	N of Bir Al Ghazal	Sandstone	10	A13	65.58	0.34	0.72	2.86	2.57
	N of Bir Al Ghazal	Sandstone	11	A14	79.13	0.42	5.65	2.92	2.63
	S of Bir Qadqud	Claystone	12	A15	62.95	1.52	22.22	1.33	1.20
	NW of Qaydam	Sandstone	13	A16	66.70	0.84	3.62	2.91	2.62
	WNW of Quttah	Sandstone	14	A17	99.02	0.07	0.21	0.12	0.11
	E of Quttah	Claystone	15	A18	50.35	1.69	29.24	2.25	2.02
	WSW of Khasm An Niqwi	Claystone	16	A19	57.50	1.77	24.72	3.03	2.73
	NNW of Dabdab	Ironstone	17	A20	16.48	0.55	7.59	62.86	56.56
	WSW of Khasm An Niqwi	Ironstone	18	A21	18.37	0.51	9.41	51.33	46.19
	WSW of Khasm An Niqwi	Sandstone	19	A22	66.03	1.00	2.86	15.51	13.96
	NW of Aqar	Conglomerate	20	A23	17.62	0.12	3.86	16.00	14.40
	WSW of Tarut	Claystone	22	A24	48.33	1.13	30.28	1.86	1.67
	WSW of Tarut	Claystone	23	A25	49.18	1.31	32.67	2.28	2.05
	WSW of Bir Al Ghazal	Siltstone	24	A26	84.00	1.64	8.82	1.71	1.54
	N of Bir Al Ghalmayah	Ironstone	25	A27	15.97	0.65	6.00	49.18	44.25
	SW of Quttah	Sandstone	26	A28	52.87	0.32	3.15	12.96	11.66
	WSW of Tarut	Ironstone	27	A29	22.70	0.76	14.45	43.41	39.06
	WSW of Tarut	Ironstone	28	A30	20.86	0.51	11.33	46.59	41.92
	E of Quttah	Claystone	29	A31	50.99	1.66	26.76	7.00	6.30
	N of Bir Al Ghalmayah	Claystone	30	A32	47.89	1.11	32.42	3.32	2.99
	SE of Bir Al Ghazal	Sandstone	31	A33	82.89	1.65	7.72	1.45	1.30
	NE of Bir Al Ghalmayah	Sandstone	32	A34	90.52	0.56	2.76	3.65	3.28
	NNW of Qarat Al Baddadah	Ironstone	33	A35	18.57	0.39	5.15	48.35	43.51
	N of Ash Shab	Ironstone	34	A36	11.42	0.39	6.03	44.48	40.02
	NE of Bir Al Ghalmayah	Ironstone	35	A37	10.30	0.21	5.30	61.27	55.13
	SW of Bir Al Ghazal	Ironstone	36	A38	25.27	1.32	5.52	58.41	52.56
Al Fuqaha	SW of Qarqaf Al Aqwaz	Sandstone	9	A39	69.98	0.26	2.64	20.08	18.07
	S of Qarqaf Al Aqwaz	Sandstone	10	A40	54.00	0.31	1.41	39.05	35.14
	SSW of Qarqaf Al Aqwaz	Ironstone	11	A41	6.49	0.52	5.06	67.04	60.32

Table 1: Continued

Sheet	Area	Lithology	Sample No. in the sheets	Sample No. in this work	MnO	MgO	CaO	Na_2O
Idri	W of Idri	Ironstone	1	A1	1.09	0.36	0.97	0.33
	SW of Wanzarik	Sandstone	37	A2	0.12	0.10	0.61	0.20
	NE of Bir Al Qasr	Ironstone	26	A3	0.49	0.86	1.25	6.73
	ESE of Wanzarik	Sandstone	31	A4	0.02	0.10	0.44	0.14
	Wadi Ash Shati	Ironstone	39	A5	3.52	0.36	20.23	0.97
	Wadi Ash Shati	Ironstone	40	A6	6.17	0.55	5.35	0.48
	Wadi Ash Shati	Ironstone	43	A7	0.33	1.74	1.91	0.62
	Wadi Ash Shati	Ironstone	44	A8	0.59	2.84	4.60	1.51
Sabha	NE of Bargan	Claystone	6	A9	0.07	0.92	0.87	1.50
	Quwir Al Ghanaim	Sandstone	7	A10	0.04	0.10	0.15	0.15
	SE of Bargan	Sandstone	8	A11	0.01	0.10	0.15	0.11
	W of Al Qarat Al Bayda	Sandstone	9	A12	0.13	0.36	0.65	0.50
	N of Bir Al Ghazal	Sandstone	10	A13	19.92	0.17	1.96	0.11
	N of Bir Al Ghazal	Sandstone	11	A14	0.27	2.20	0.46	0.90
	S of Bir Qadqud	Claystone	12	A15	0.00	0.43	0.33	0.15
	NW of Qaydam	Sandstone	13	A16	21.20	0.12	0.01	0.22
	WNW of Quttah	Sandstone	14	A17	0.00	0.08	0.15	0.11
	E of Quttah	Claystone	15	A18	0.06	0.68	0.18	1.50
	WSW of Khasm An Niqwi	Claystone	16	A19	0.02	0.33	0.18	1.20
	NNW of Dabdab	Ironstone	17	A20	4.41	0.19	0.45	0.07
	WSW of Khasm An Niqwi	Ironstone	18	A21	3.37	0.14	1.45	0.08
	WSW of Khasm An Niqwi	Sandstone	19	A22	0.22	0.15	6.41	0.14
	NW of Aqar	Conglomerate	20	A23	1.14	0.61	27.95	0.10
	WSW of Tarut	Claystone	22	A24	0.01	0.56	0.31	1.20
	WSW of Tarut	Claystone	23	A25	0.01	0.45	0.14	0.20
	WSW of Bir Al Ghazal	Siltstone	24	A26	0.10	0.10	0.18	0.15
	N of Bir Al Ghalmayah	Ironstone	25	A27	1.16	0.41	9.18	0.10
	SW of Quttah	Sandstone	26	A28	18.75	0.57	0.35	0.78
	WSW of Tarut	Ironstone	27	A29	0.28	1.17	1.12	2.12
	WSW of Tarut	Ironstone	28	A30	0.51	2.47	3.44	0.45
	E of Quttah	Claystone	29	A31	0.00	0.46	0.12	0.44
	N of Bir Al Ghalmayah	Claystone	30	A32	0.01	0.25	0.23	0.50
	SE of Bir Al Ghazal	Sandstone	31	A33	0.08	0.10	1.02	0.07
	NE of Bir Al Ghalmayah	Sandstone	32	A34	0.05	0.10	0.12	0.09
	NNW of Qarat Al Baddadah	Ironstone	33	A35	0.41	0.23	5.42	0.21
	N of Ash Shab	Ironstone	34	A36	0.00	0.26	13.12	0.44
	NE of Bir Al Ghalmayah	Ironstone	35	A37	0.59	0.24	2.35	0.60
	SW of Bir Al Ghazal	Ironstone	36	A38	0.75	0.10	0.08	0.21
Al Fuqaha	SW of Qarqaf Al Aqwaz	Sandstone	9	A39	0.07	0.24	1.45	0.10
	S of Qarqaf Al Aqwaz	Sandstone	10	A40	0.08	0.15	0.27	0.05
	SSW of Qarqaf Al Aqwaz	Ironstone	11	A41	0.35	0.43	2.47	0.25

Table 1: Continued

Sheet	Area	Lithology	Sample No. in the sheets	Sample No. in this work	K_2O	P_2O_5	SO_3	LOI
Idri	W of Idri	Ironstone	1	A1	0.21	0.46	2.39	10.22
	SW of Wanzarik	Sandstone	37	A2	0.11	0.12	0.35	1.20
	NE of Bir Al Qasr	Ironstone	26	A3	1.15	0.55	0.99	13.62
	ESE of Wanzarik	Sandstone	31	A4	0.09	0.04	0.08	0.60
	Wadi Ash Shati	Ironstone	39	A5	0.47	5.80	2.90	9.87
	Wadi Ash Shati	Ironstone	40	A6	0.50	2.91	1.77	8.26
	Wadi Ash Shati	Ironstone	43	A7	0.34	1.28	1.18	9.57
	Wadi Ash Shati	Ironstone	44	A8	0.77	2.80	0.46	12.31
Sabha	NE of Bargan	Claystone	6	A9	1.75	0.23	0.13	13.70
	Quwir Al Ghanaim	Sandstone	7	A10	0.11	0.07	0.20	0.50
	SE of Bargan	Sandstone	8	A11	0.07	0.03	0.09	0.50
	W of Al Qarat Al Bayda	Sandstone	9	A12	0.33	0.07	0.70	1.70
	N of Bir Al Ghazal	Sandstone	10	A13	1.03	0.39	0.52	5.97
	N of Bir Al Ghazal	Sandstone	11	A14	1.20	0.05	0.32	6.40
	S of Bir Qadqud	Claystone	12	A15	1.65	0.11	0.33	8.49
	NW of Qaydam	Sandstone	13	A16	0.37	0.18	0.01	4.00
	WNW of Quttah	Sandstone	14	A17	0.05	0.02	0.01	0.41
	E of Quttah	Claystone	15	A18	1.21	0.12	0.38	12.80
	WSW of Khasm An Niqwi	Claystone	16	A19	0.93	0.13	0.15	10.00
	NNW of Dabdab	Ironstone	17	A20	0.17	0.91	0.16	6.26
	WSW of Khasm An Niqwi	Ironstone	18	A21	0.36	3.29	0.65	11.20
	WSW of Khasm An Niqwi	Sandstone	19	A22	0.35	1.99	0.30	5.20
	NW of Aqar	Conglomerate	20	A23	0.17	25.00	0.77	6.80
	WSW of Tarut	Claystone	22	A24	1.38	0.25	0.95	14.20
	WSW of Tarut	Claystone	23	A25	1.25	0.12	0.18	12.50
	WSW of Bir Al Ghazal	Siltstone	24	A26	0.32	0.13	0.05	2.80
	N of Bir Al Ghalmayah	Ironstone	25	A27	0.30	7.69	1.97	7.78
	SW of Quttah	Sandstone	26	A28	1.23	0.48	0.37	7.67
	WSW of Tarut	Ironstone	27	A29	1.05	0.19	0.02	12.04
	WSW of Tarut	Ironstone	28	A30	0.51	3.13	0.25	10.00
	E of Quttah	Claystone	29	A31	1.80	0.14	0.01	10.14
	N of Bir Al Ghalmayah	Claystone	30	A32	0.59	0.24	0.03	13.10
	SE of Bir Al Ghazal	Sandstone	31	A33	0.26	0.07	1.07	3.60
	NE of Bir Al Ghalmayah	Sandstone	32	A34	0.96	0.13	0.07	1.10
	NNW of Qarat Al Baddadah	Ironstone	33	A35	0.14	8.30	1.88	11.20
	N of Ash Shab	Ironstone	34	A36	0.25	11.61	2.65	9.77
	NE of Bir Al Ghalmayah	Ironstone	35	A37	0.12	0.76	5.43	13.30
	SW of Bir Al Ghazal	Ironstone	36	A38	0.36	1.51	0.01	6.70
Al Fuqaha	SW of Qarqaf Al Aqwaz	Sandstone	9	A39	0.25	0.27	0.80	3.70
	S of Qarqaf Al Aqwaz	Sandstone	10	A40	0.02	0.36	0.65	3.55
	SSW of Qarqaf Al Aqwaz	Ironstone	11	A41	0.12	1.16	3.30	12.81

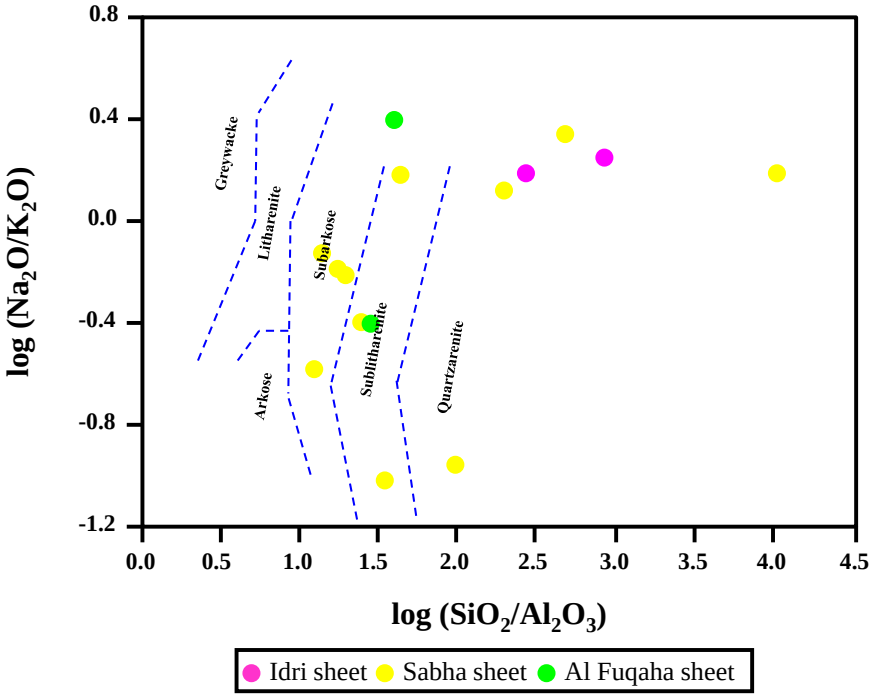

Fig. 4: Binary plot of log (SiO_2/Al_2O_3) vs. log (Na_2O/K_2O) showing the classification of the studied sandstones (fields after Pettijohn et al., 1972).

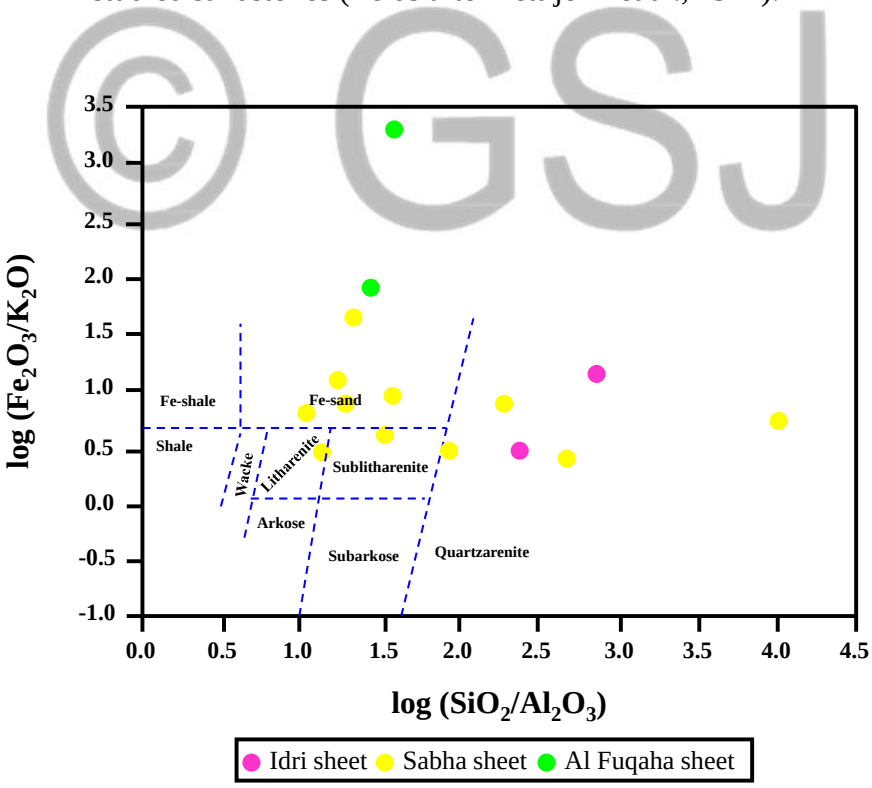

Fig. 5: Binary plot of log (SiO_2/Al_2O_3) vs. log (Fe_2O_3/K_2O) showing the classification of the studied sandstones (fields after Herron, 1988).

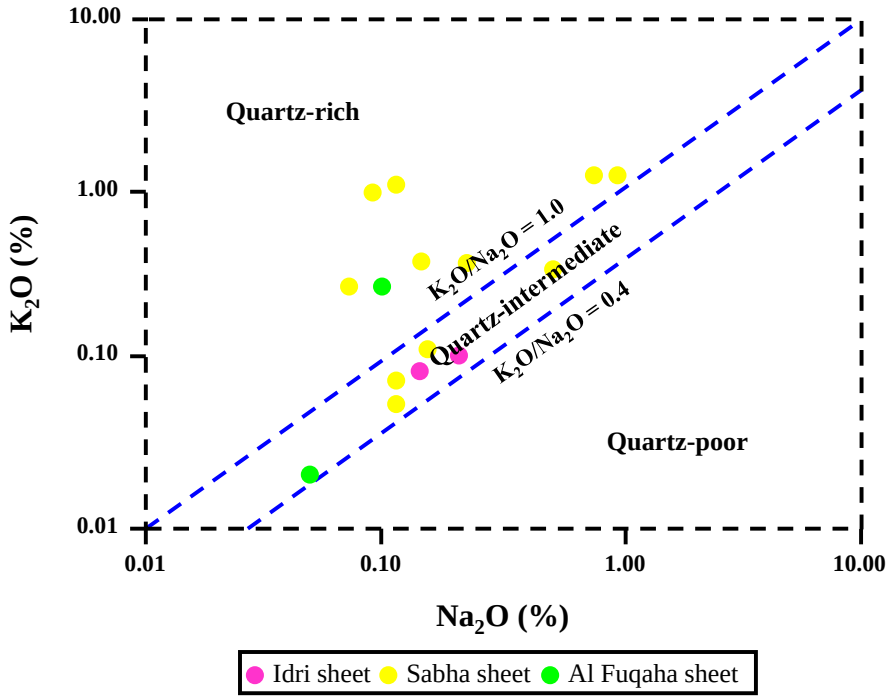

Fig. 6: Binary plot of Na_2O vs. K_2O showing the classification of the studied sandstones (fields after Crook, 1974).

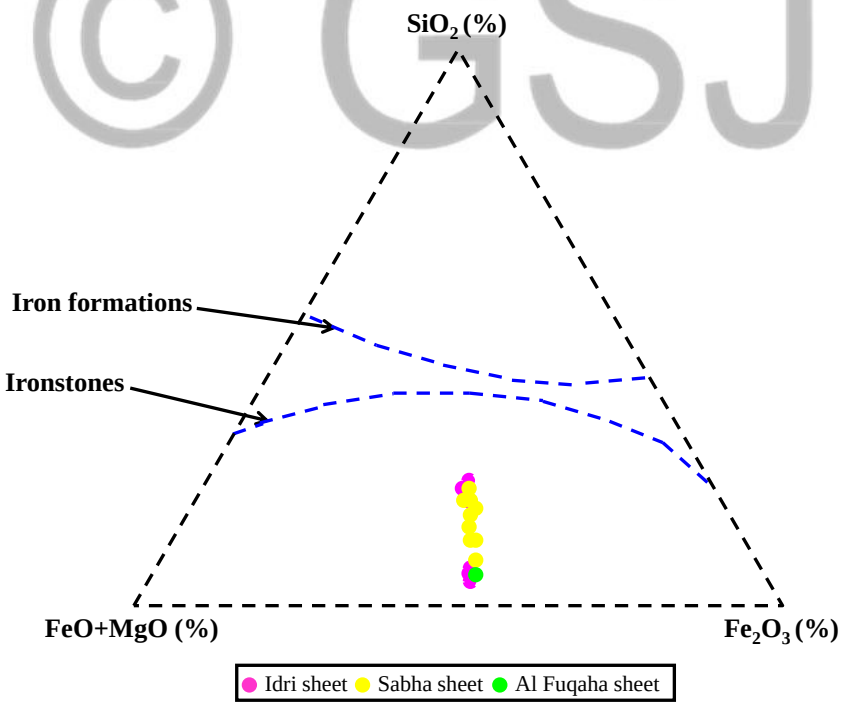

Fig. 7: Ternary plot of SiO_2-FeO+MgO-Fe_2O_3 showing the difference between Phanerozoic ironstones and Precambrian iron formations (fields after James, 1992).

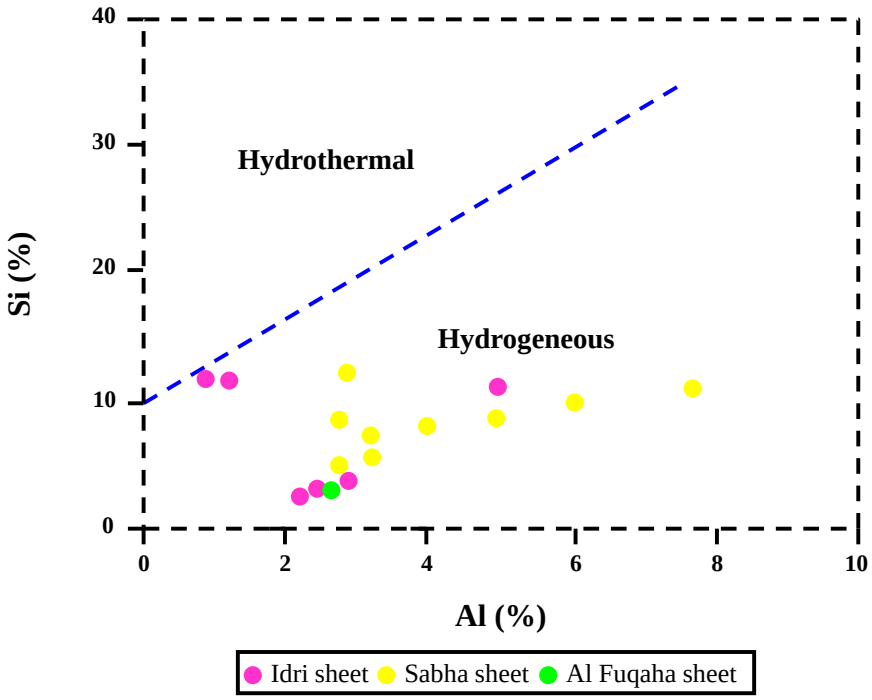

Fig. 8: Binary plot of Al vs. Si showing the origin of the studied ironstones (fields after Choi and Hariya, 1992).

5.2. Normalization

Several sedimentary rocks are used for normalization, such as the Post Archean Australian Shale (PAAS, Taylor and McLennan, 1985) and the North American Shale Composite (NASC, Gromet et al., 1984). The PAAS values were utilized to standardize the chemical composition of the examined samples. As a result of the difference in the rock types, the normalized data (Fig. 9) show clear differences in enrichment and depletion.

5.3. Provenance

Determining the parent rock of the sediments, the age of deposition, and the paleoclimate are the main goals of the provenance research. The provenance of clastic rocks have been determined using the chemical composition (Nagarajan et al., 2007). The Al_2O_3/TiO_2 ratio is obviously different in felsic (21-70), intermediate (8-21) and mafic (3-8) rocks (Hayashi et al., 1997). In the studied rocks, the Al_2O_3/TiO_2 ratio ranges from 0.06 to 32.17, which indicates that there is a mixed source for the Awainat Wanin Formation. Further evidence supporting this assumption can be found in the binary plot of Al_2O_3 versus TiO_2 (Fig. 10) and the ternary plot of Si/10-CaO*-MgO-Na_2O+K_2O (Fig. 11). Based on the values of the major oxides in felsic, intermediate, and mafic

rocks, the author proposed a new discrimination diagram (CaO versus Na_2O, Fig. 12) to determine the provenance of clastic sediments. This diagram shows additional indication of the mixed source. The author believes that the possible provenance of the Awainat Wanin Formation are the felsic (granite, pegmatite, aplite, and granodiorite), intermediate (andesite), and mafic (dolerite) rocks found in the Al Haruj Al Abyad Sheet (Fig. 2).

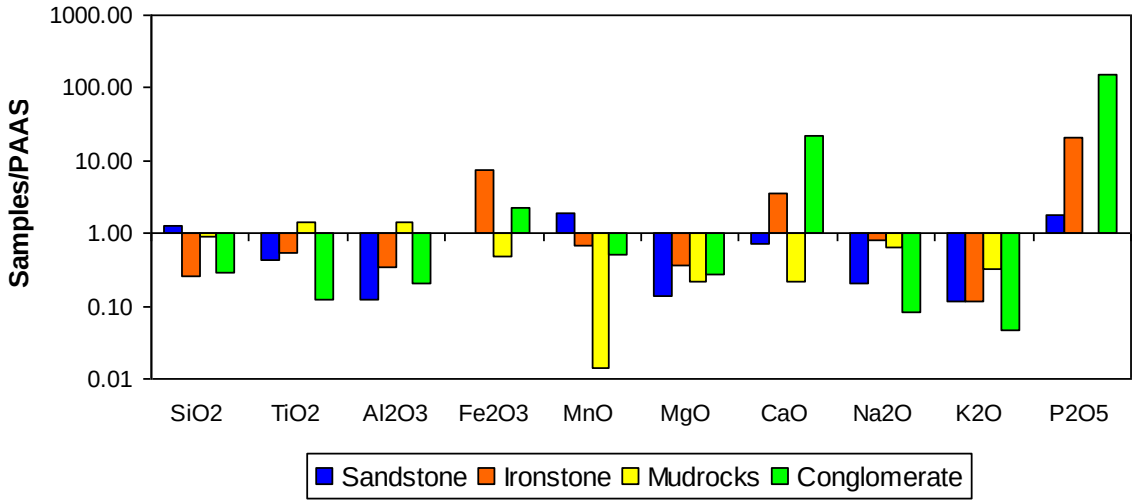

Fig. 9: Major oxides content of the Awainat Wanin Formation normalized to the PAAS.

5.4. Paleoweathering

Chemical index of alteration (CIA = $(Al_2O_3/(Al_2O_3+CaO^*+Na_2O+K_2O))100$, Nesbitt and Young, 1982), chemical index of weathering (CIW = $(Al_2O_3/(Al_2O_3+CaO^*+Na_2O))100$, Harnois, 1988), plagioclase index of alteration (PIA = $((Al_2O_3–K_2O)/((Al_2O_3–K_2O)+CaO^*+ Na_2O))100$, Fedo et al., 1995), modified version of chemical index of weathering (CIW´ = $(Al_2O_3/(Al_2O_3+ Na_2O))100$, Cullers, 2000), and ternary plot of Al_2O_3-(Na_2O+CaO*)-K_2O (A-CN-K, Nesbitt and Young, 1982) are the main techniques used to evaluate paleoweathering in the source area. CaO* expresses the concentration of CaO in the silicate fraction. CaO* can be calculated using the concentrations of CaO, P_2O_5 and Na_2O. If $Na_2O>CaO-P_2O_5$, then CaO* = $CaO-P_2O_5$, while if $Na_2O<CaO-P_2O_5$, then CaO* = Na_2O (McLennan et al., 1993). There are five classes of CIA: (1) Very slightly weathered (50-60%); (2) Slightly weathered (60-70%); (3) Moderately weathered (70-80%); (4) Highly weathered (80-90%); and (5) Extremely weathered (90-100%) (Nesbitt and Young, 1982). The values of CIA (3.33-96.72%), CIW (4.35-99.33%), PIA (2.44-99.3%), and CIW´ (8.33-99.39%) show a noticeable variance. It should be noted that only five samples (samples A2, A8, A11, A13, and A17) have CIA values less than 50%. The values in the other samples range from

51.95 to 96.72%, indicating that the source area experienced very slight to extreme weathering. Corroborating the assumption is the ternary plot of A-CN-K (Fig. 13).

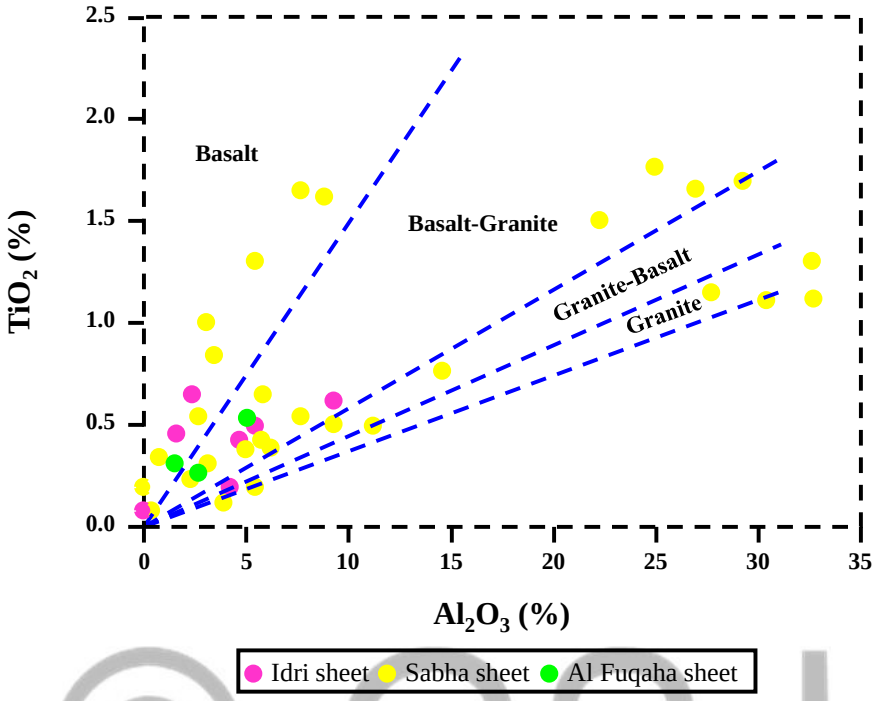

Fig. 10: Binary plot of Al_2O_3 vs. TiO_2 showing the provenance of the Awainat Wanin Formation (fields after Hayashi et al., 1997).

5.5. Paleoclimate

Paleoclimate and the movement elements of humid climate (Fe and Mn) and arid climate (Ca, Mg, K, and Na) are closely related (Khan et al., 2023). The CIA can be used to assess the paleoclimatic conditions (Nesbitt and Young, 1982). The typical CIA values for arid climate, temperate climate, and humid climate are <70%, 70-80%, and 80-100%, respectively. The binary plot of $Al_2O_3+K_2O+Na_2O$ versus SiO_2 (Fig. 14) was utilized to evaluate the paleoclimate in the source area. Evidently, there were fluctuations in both humidity and aridity during the deposition. The preceding assumption is supported by the distinct variation in the CIA (3.33-96.72%), Ti/Al (0.04-20.38), Mg/Al (0.01-11.35), and Fe/Al (0.08-45.38) values.

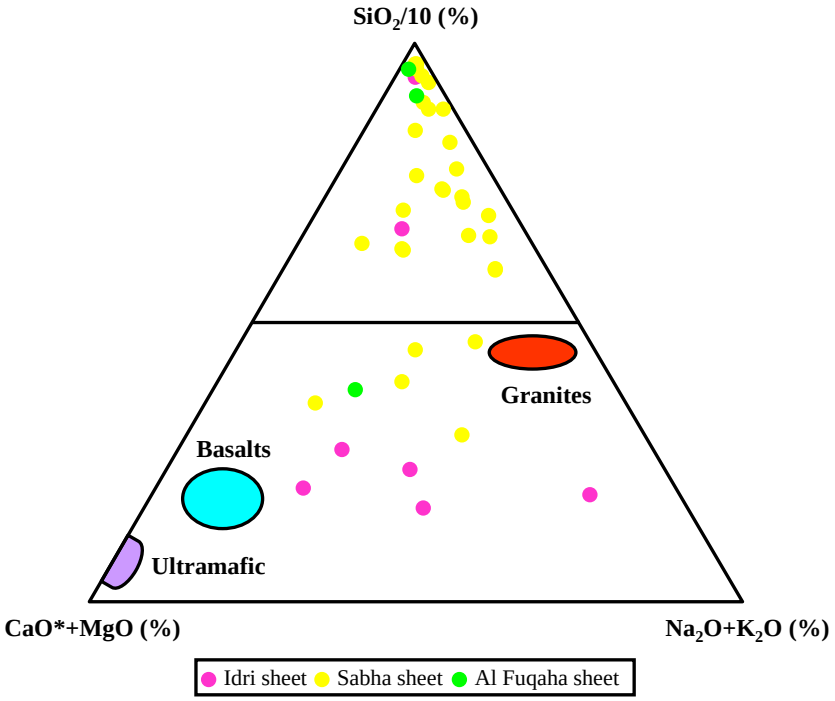

Fig. 11: Ternary of Si/10-CaO*-MgO-Na_2O+K_2O showing the provenance of the Awainat Wanin Formation (fields after Taylor and McLennan, 1985).

5.6. Maturity

According to Cox et al., (1995) the index of compositional variability (ICV = (Fe_2O_3+K_2O+Na_2O+CaO*+MgO+MnO+TiO_2)/Al_2O_3) can be used to evaluate the maturity of sediments. Immature sediments are indicated by high values (ICV>1, tectonically active environment), while low values (ICV<1, tectonically quiescent setting) suggest a mature sediment (Goldberg and Humayun, 2010). The distinct variance observed in the ICV values (0.17-91) suggests the existence of both immature and mature sediments.

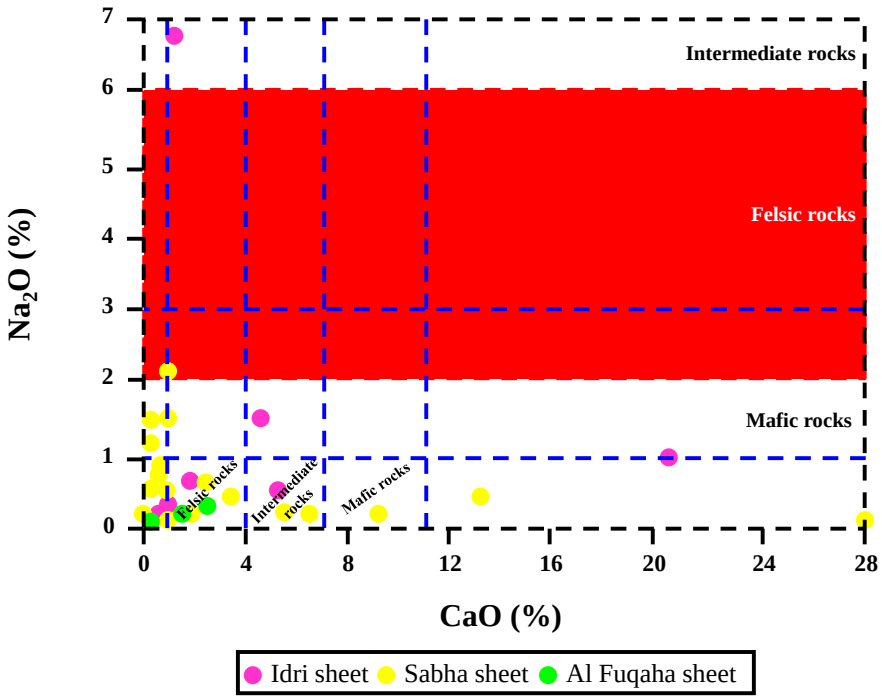

Fig. 12: Binary plot of CaO vs. Na_2O showing the provenance of the Awainat Wanin Formation (proposed by the author).

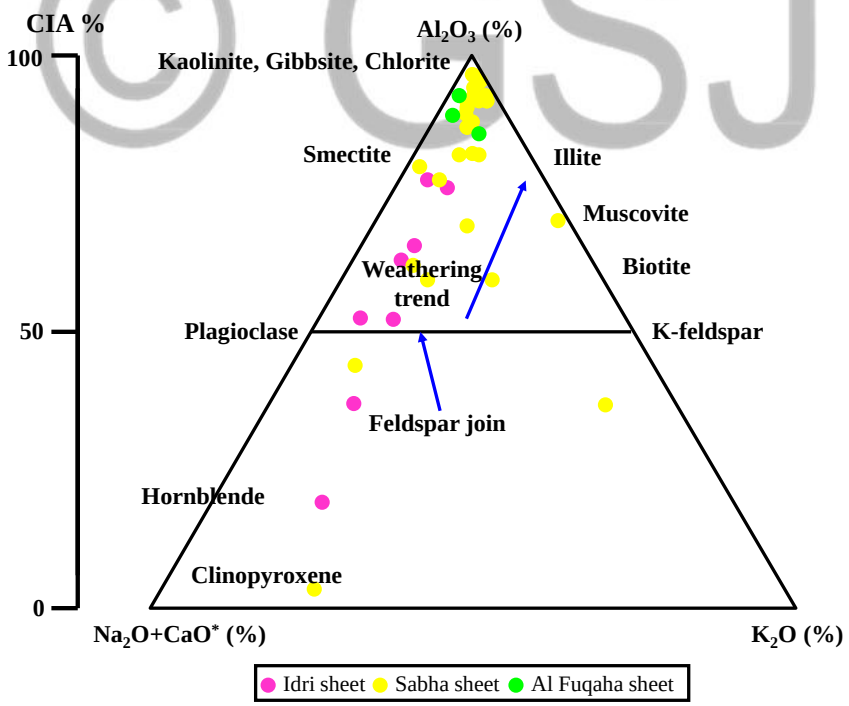

Fig. 13: Ternary plot of A-CN-K showing the paleoweathering intensity in the source area (fields after Nesbitt and Young, 1982).

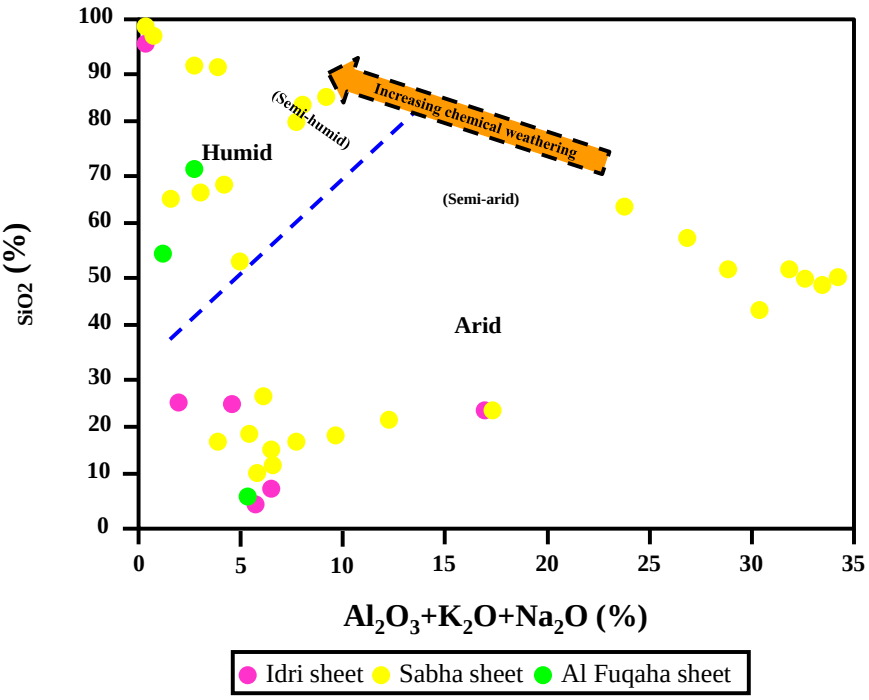

Fig. 14: Binary plot of $Al_2O_3+K_2O+Na_2O$ vs. SiO_2 showing the paleoclimate conditions in the source area (fields after Suttner and Dutta, 1986).

5.7. Depositional Environment

Fossils, chemical composition, sedimentary facies, and sedimentary structures are used to identify the depositional environment in ancient sediments. The Awainat Wanin Formation's confirmed depositional setting is the deltaic environment (Vos, 1981), as the author stated early in this work. The hypothesis of Vos (1981) is supported by the binary plot of MgO versus FeO (Fig. 15), and the ternary plot of $MgO-Fe_2O_3-SiO_2/Al_2O_3$ (Fig. 16). Paleosalinity may have an impact on the stratification of water bodies, which may have an impact on the level of paleoproductivity and organic matter preservation (Chen et al., 2020). Changes in rainfall and evaporation may have a direct impact on changes in water bodies' salinity. For this reason, paleosalinity can, to some extent, reflect paleoclimate change (Algeo and Maynard, 2004). Ca/(Ca+Fe) is a widely used geochemical proxy that exhibits high reliability in reflecting variations in water salinity over geologic time (Zhang et al., 2013). The standard Ca/(Ca+Fe) ratios for saline water, brackish water, and fresh water are 0.8, 0.4-0.8, and <0.4, respectively (Khan et al., 2023). The Ca/(Ca+Fe) ratios in this study (0.001-0.64) indicate that water changed from brackish to fresh during deposition.

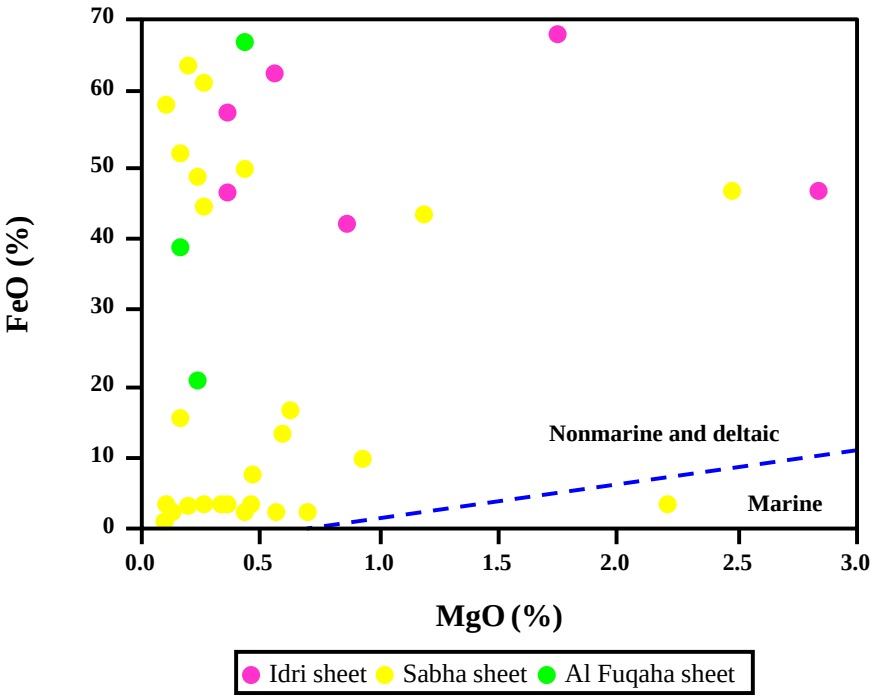

Fig. 15: Binary plot of MgO vs. FeO showing the depositional environment of the Awainat Wanin Formation (fields after Ratcliffe et al., 2007).

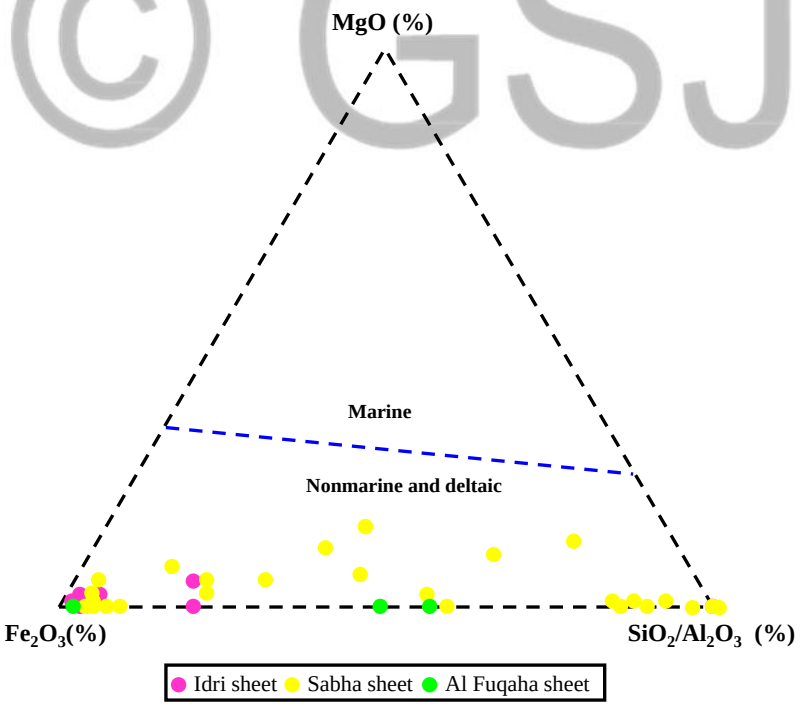

Fig. 16: Ternary plot of MgO-Fe_2O_3-SiO_2/Al_2O_3 showing the depositional environment of the Awainat Wanin Formation (fields after Ratcliffe et al., 2007).

The paleoredox conditions are determined by a number of parameters including Mn* (Machhour et al., 1994; Bellanca et al., 1996). The formula for calculating Mn* is as follows: Mn* =

$\log((Mn_{sample}/Mn_{shale})/(Fe_{sample}/Fe_{shale}))$. Wedepohl (1978) states that the mean values for Fe_{shale} and Mn_{shale} are 46150 ppm and 600 ppm, respectively. It should be noted that Mn* is not calculated for samples A15, A17, A31 and A36, because Mn is not detected in these samples. The Mn* values (−0.76-2.79) indicate that suboxic conditions prevailed during the deposition of the Awainat Wanin Formation.

5.8. Paleoproductivity

The distribution and formation of source rocks are significantly influenced by paleoproductivity, which is primarily determined by the availability of nutrient elements. Consequently, the analysis of paleoproductivity is often based on P concentration. Evaluation of paleoproductivity can be done using several parameters such as P/Ti ratio (Canfield, 1994). According to Yang et al., (2022) high values of P/Ti ratio (>0.79) suggest high paleoproductivity, low values (<0.34) reveal low paleoproductivity, and values between 0.34 and 0.79 indicate medium paleoproductivity. The Awainat Wanin Formation exhibits a wide range of paleoproductivity (from low to high), as indicated by the P/Ti ratio (0.03-152.78).

5.9. Paleotectonic Setting

Numerous investigations have demonstrated that the paleotectonic settings of the provenance and depositional environment of clastic rocks have a major influence on the chemical composition (e.g., Roser and Korsch, 1986). The binary plot of SiO_2 versus K_2O/Na_2O (Fig. 17) distinguishes between oceanic island arc, active continental margin and passive margin. Clearly, the data of the Awainat Wanin Formation fall in the fields of active continental margin and passive margin (except for samples A9, A18, and A40).

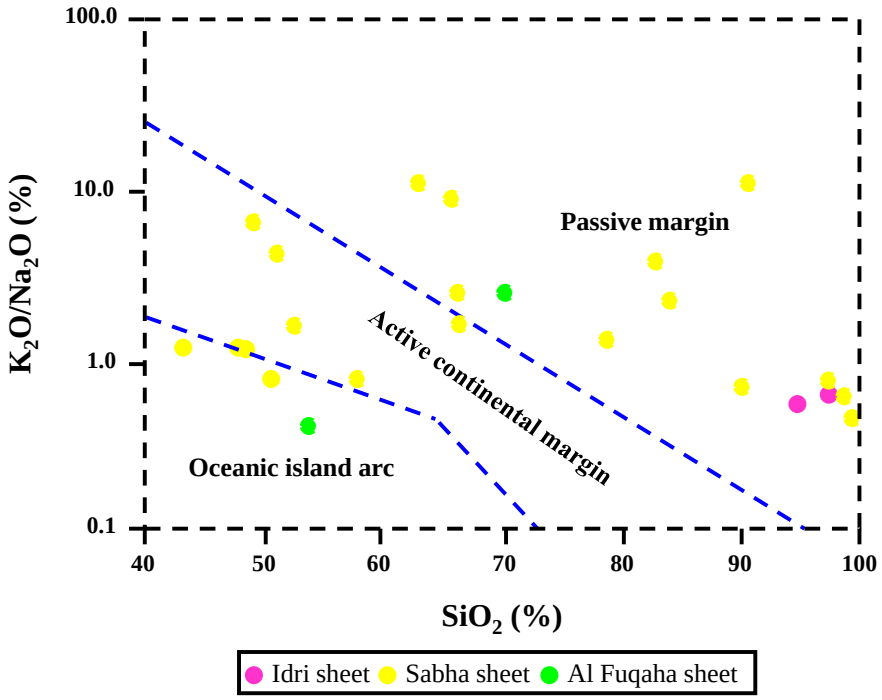

Fig. 17: Binary plot of SiO_2 vs. K_2O/Na_2O showing the paleotectonic setting of the Awainat Wanin Formation (fields after Roser and Korsch, 1986).

6. Conclusions

The following are the work's primary conclusions:

1) The sandstones of the Idri Sheet are classified as quartzarenite, those of the Sabha Sheet are divided into litharenite, sublitharenite, subarkose, and quartzarenite, and the Al Fuqaha Sheet contains subarkose and sublitharenite.

2) Clinton variety is the confirmed type of the ironstones. Their primary origin is hydrogenous.

3) The conglomerate (bone bed) belongs to the phosphorite rocks.

4) There were different sources for the Awainat Wanin Formation. The felsic, intermediate, and mafic rocks present in the Al Haruj Al Abyad Sheet may be the source of the formation.

5) There was variation in the weathering intensity in the source area from very slight to extreme.

6) The paleoclimate in the source area fluctuated from humid to arid.

7) The formation contains immature and mature sediments.

8) The verified depositional setting is the deltaic environment (suboxic conditions). The water altered from brackish to fresh throughout the deposition.

9) The paleoproductivity varies widely.

10) Active continental margin and passive margin are the confirmed paleotectonic settings.

References

Aboglila, S., Elaalem, M., Ezlit, Y. and Farifr, E. (2018): Geochemical characteristics of six formations based on organic geochemical parameters, Murzuq Basin, Libya. Advances in Research; 15(4): 1-11.

Algeo, T.J. and Maynard, J.B. (2004): Trace-element behavior and redox facies in core shales of Upper Pennsylvanian Kansas-type cyclothems. Chemical Geology; 206: 289-318.

Aziz, A. (2000): Stratigraphy and hydrocarbon potential of the Lower Palaeozoic succession of License NC-115, Murzuq Basin, SW Libya. In Sola, M.A. and Worsley, D. (eds) Geological Exploration in Murzuq Basin. Elsevier, Amsterdam; pp. 349-368.

Basal, A.M.K., Sarhan, M.A., Alfarog, M.G., Eltwargy, E. and El Bahrawy, A. (2023): Well Logging analysis of the Devonian Awaynat Wanin Formation (F3) "B" in A37-NC169a well, Al Wafa field, Ghadames Basin, Libya. Scientific Journal for Damietta Faculty of Science, 13(1): 83-89.

Belhaj, A.F., El Gheriani, M. and Targhi, M.H. (2021): Sedimentology and petrophysics of upper Devonian F3 sandstone Wafa filed (NC-169) Ghadames basin-south west Libya. University Bulletin; 3(23): 167-190.

Bellanca, A., Claps, M., Erba, E., Masetti, D., Neri, R., Premoli-Silva, I. and Venezia, F. (1996): Orbitally induced limestone/marlstone rhythms in the Albian-Cenomanian Cismon section (Venetian región, northern Italy): sedimentology, calcareous and siliceous plankton distribution, elemental and isotope geochemistry. Palaeogeography, Palaeoclimatology, Palaeoecology; 126: 227-260.

Blanpied, C. and Rubino, J.L. (1997): Fieldwork report. Gargaf area. Libya. Confidential TOTAL Report, Tripoli; 33p.

Canfield, D.E. (1994): Factors influencing organic carbon preservation in marine sediments. Chemical Geology; 114: 315-329.

Chen, G., Gang, W., Chang, X., Wang, N., Zhang, P., Cao, Q. and Xu, J. (2020): Paleoproductivity of the Chang 7 unit in the Ordos Basin (North China) and its controlling factors. Palaeogeography, Palaeoclimatology, Palaeoecology; 551: 109741.

Choi, J.H. and Hariya, Y. (1992): Geochemistry and depositional environment of Mn oxide deposits in the Tokoro Belt, Northeastern Hokkaido. Economic Geology: 87(5): 1265-1274.

Collomb, G.R. (1962): Etude geologique du Jebel Fezzan et de sa bordure Paleozoique. Notes et Mém. Comp. Fr. Pétrol., 1: 7-35.

Cox, R., Low, D.R. and Cullers, R.L. (1995): The influence of sediment recycling and basement composition on evolution of mudrock chemistry in the southwestern United States. Geochimica et Cosmochimica Acta; 59: 2919-2940.

Crook K.A.W. (1974): Lithogenesis and geotectonics: The significance of compositional variation in flysch arenites (greywackes). Society for Sedimentary Geology Special Publication (SEPM); 19: 304-310.

Cullers, R.L. (2000): The geochemistry of shales, siltstones, and sandstones of Pennsylvanian-Permian age, Colorado, USA: Implication for provenance and metamorphic studies. Lithos; 51: 181-203.

Echikh, K. (1998): Geology and hydrocarbon occurrences in the Ghadames Basin, Algeria, Tunisia, Libya. In MacGregor, D.S., Moody, R.T.J. and Clark-Lowes, D.D. (eds) Petroleum Geology of North Africa. Geological Society, London, Special Publications; 132: 109-129.

Evans, A.M. (1993): Ore geology and industrial minerals: An introduction. 3rd edition, Wiley-Blackwell; 400p.

Fedo, C.M.; Nesbitt, H.W. and Young, G.M. (1995): Unraveling the effects of potassium metasomatism in sedimentary rocks and paleosols, with implications for paleoweathering conditions and provenance. Geology; 23: 921-924.

Goldberg, K. and Humayun, M. (2010): The applicability of the Chemical Index of Alteration as a paleoclimatic indicator: An example from the Permian of the Paraná Basin, Brazil. Palaeogeography, Palaeoclimatology, Palaeoecology; 293: 175-183.

Gromet, L.P., Dymek, R.F., Haskin, L.A. and Korotev, R.L. (1984): The North American Shale Composite: Its compilation, major and trace element characteristics. Geochimica et Cosmochimica Acta; 48: 2469-2482.

Hallett, D. (2002): Petroleum geology of Libya. Amsterdam, Elsevier Inc., 503p.

Harnois, L. (1988): The CIW index: A new chemical index of weathering. Sedimentary Geology; 55: 319-322.

Hayashi, K., Fujisawa, H., Holland, H. and Ohmoto, H. (1997): Geochemistry of ~1.9 Ga sedimentary rocks from northeastern Labrador, Canada. Geochimica et Cosmochimica Acta; 61(19): 4115-4137.

Herron, M.M. (1988): Geochemical classification of terrigenous sandstone and shale from core and log data. Journal of Sedimentary Petrology; 5(8): 820-829.

Jabir, A., Cerepi, A., Loisy, C. and Rubino, J.-L. (2021): Evaluation of reservoir systems in Paleozoic sedimentary formations of Ghadames and Jefarah basins. Journal of African Earth Sciences; 183: 104324.

James, H.L. (1992): Precambrian iron-formations: Nature, origin, and mineralogic evolution from sedimentation to metamorphism. In Wolf, K.H. and Chilingarian, G.V. (eds), Diagenesis: III. Developments in Sedimentology; 47: 543-589.

Khan, K.F., Dar, S.A., and Khan, S.A. (2012): Geochemistry of phosphate bearing sedimentary rocks in parts of Sonrai block, Lalitpur District, Uttar Pradesh, India. Geochemistry; 72(2): 117-125.

Khan, D., Zijun, L., Qiu, L., Kuiyuan, L., Yongqiang, Y., Cong, N., Bin, L., Li, X. and Habulashenmu, Y. (2023): Mineralogical and geochemical characterization of lacustrine calcareous shale in Dongying Depression, Bohai Bay Basin: Implications for paleosalinity, paleoclimate, and paleoredox conditions. Geochemistry, In Press.

Lelubre, M. (1946): Sur le paléozoique du Fezzan. Com. Rend. Hebd. Séanc. Acad. Sci.; 222: 1403-1404.

Machhour, L., Philip, J. and Oudin, J.L. (1994): Formation of laminate deposits in anaerobic-dysaerobic marine environments. Marine Geology; 117: 287-302.

Massa, D. and Collomb, G.R. (1960): Observations nouvelles sur la region d'Aouinet Ouenine et du Djebel Fezzan (Libye). 21st International Geological Congress Proceedings. Copenhagen; 12: 65-73.

Massa, D. and Moreau-Benoit, A. (1976): Essai de synthese stratigraphique et palynologique du system Devonien en Libye occidentale. Rev. Inst. Fr. Petrol., 31: 287-332.

McClellan, G.H. and Gremillion, L.R. (1980): Evaluation of phosphate raw materials. In Khasawneh chairman, F.E., Sample, E.C. and Kamprath, E.J. (eds), The role of phosphorus in agriculture. American Society of Agronomy, Madison, Wisconsin; pp. 42-80.

McLennan, S.M., Hemming, S., McDaniel, D.K. and Hanson, G.N. (1993): Geochemical approaches to sedimentation, provenance, and tectonics. In Johnson, M.J. and Basu, A. (eds), Processes Controlling the Composition of Clastic Sediments: Geological Society of America, Special Paper; 284: 21-40.

Miles, N.H. (2001): A palynological correlation of the Palaeozoic. Robertson Research International, Confidential ROO Report No 6204/Ib., 95p.

Mohamed, K.H., Albaghdady, A.A., Abdullah, M. and Abduallah, S. (2017): Facies analysis of Lower Awynat Wanin formations in Murzuq Basin, SW of Libya. Journal of Pure and Applied Science; 16(2): 56-67.

Morton, A.C., Meinhold, G., Howard, J.P., Phillips, R.J., Strogen, D., Abutarruma, Y., Elgadry, M., Thusu, B. and Whitham, A.G. (2011): A heavy mineral study of sandstones from the eastern Murzuq Basin, Libya: Constraints on provenance and stratigraphic correlation. Journal of African Earth Sciences; 61(4): 308-330.

Nagarajan, R., Madhavaraju, J., Nagendra, R., Armstrong-Altrin, J.S. and Moutte, J. (2007): Geochemistry of Neoproterozoic shales of the Rabanpalli Formation, Bhima Basin, Northern Karnataka, southern India: implications for provenance and paleoredox conditions. Revista Mexicana de Ciencias Geológicas; 24 (2): 150-160.

Nesbitt, H.W. and Young, G.M. (1982): Early Proterozoic climates and plate motions inferred from major element chemistry of lutites. Nature; 299: 715-717.

Parizek, A., Klen, L. and Rohlich, P. (1984): Geological Map of Libya, 1:250000, Sheet: Idri, NG 33-1, Explanatory Booklet, Industrial Research Center (IRC) Tripoli, Libya; 108p.

Pettijohn, F.J. (1957): Sedimentary Rocks. 1st edition, Harper and Brothers; 718p.

Pettijohn, F.J., Potter, P.E. and Siever, R. (1972): Sand and sandstone. 1st edition, Springer New York; 583p.

Rahuma, M.M., Proust, J.N. and Eschard, R. (2007): Stratigraphic architecture of the Devonian succession in Awaynat Wanin area - Ghadamis Basin, Western Libya. 3rd EAGE North African/Mediterranean Petroleum and Geosciences Conference and Exhibition, European Association of Geoscientists and Engineers.

Ratcliffe, K.T., Morton, A.C., Ritcey, D.H. and Evenchick, C.A. (2007): Whole-rock geochemistry and heavy mineral analysis as petroleum exploration tools in the Bowser and Sustut basins, British Columbia, Canada. Bulletin of Canadian Petroleum Geology; 55(4): 320-336.

Riboulleau, A., Spina, A., Vecoli, M., Riquier, L., Quijada, M., Tribovillard, N. and Averbuch, O. (2018): Organic matter deposition in the Ghadames Basin (Libya) during the Late Devonian—A multidisciplinary approach. Palaeogeography, Palaeoclimatology, Palaeoecology; 497: 37-51.

Roser, B.P., and Korsch, R.J. (1986): Determination of tectonic setting of sandstone-mudstone suites using SiO_2 content and K_2O/Na_2O ratio. Journal of Geology; 94: 635-650.

Seidl, K. and Rohlich, P. (1984): Geological Map of Libya, 1:250000, Sheet: Sabha, NI 33-2, Explanatory Booklet. Industrial Research Centre (IRC), Tripoli, Libya; 149p.

Shalbak, F.A. (2015): Palaeozoic petroleum systems of the Murzuq Basin, Libya. Unpublished PhD Thesis, Barcelona University, Spain.

Steemans, P., Javaux, E.J., Breuer, P., Le Hérissé, A., Marshall, C.P. and De Goyet, F.D.V. (2009): Description and microscale analysis of some enigmatic palynomorphs from the middle Devonian (Givetian) of Libya. Palynology; 33: 101-112.

Sutckifte, O.E., Adamson, K. and Ben Rahuma, M.M. (2000): The Geological evolution of the Palaeozoic rocks of western Libya: A review and field guide. 2nd Symposium on the Sedimentary Basins of Libya Field Guide; 93p.

Suttner, L.J. and Dutta, P.K. (1986): Alluvial sandstone composition and paleoclimate. Framework mineralogy. Journal of Sedimentary Petrology; 56: 326-345.

Taylor, S.R. and McLennan, S.M. (1985): The continental crust: Its composition and evolution. Blackwell Scientific Publishers, Oxford; 312p.

Vos, R.G. (1981): Deltaic sedimentation in Devonian of western Libya. Sedimentary Geology; 29: 67-88.

Wedepohl, K.H. (1978): Manganese: abundance in common sediments and sedimentary rocks. In Wedepohl, K.H. (eds), Handbook of Geochemistry: Berlin, Springer; II/3: 1-17.

Woller, F. (1984): Geological Map of Libya, 1:250000. Sheet: Al Fuqaha, NG 33-3, Explanatory Booklet. Industrial Research Centre (IRC), Tripoli, Libya; 123p.

Yang, M., Zuo, Y., Fu, X., Qiu, L., Li, W., Zhang, J., Zheng, Z. and Zhang, J. (2022): Paleoenvironment of the Lower Ordovician Meitan Formation in the Sichuan Basin and adjacent areas, China. Minerals; 12(1): 75.

Zhang, M.M., Liu, Z.J., Xu, S.C., Sun, P.C. and Hu, X.F. (2013): Element response to the ancient lake information and its evolution history of argillaceous source rocks in the Lucaogou Formation in Sangonghe area of southern margin of Junggar Basin. Journal of Earth Science; 24(6): 987-996.